Separation of Intra- and Intermolecular NOEs through Simultaneous Editing and *J*-Compensated Filtering: A 4D Quadrature-Free Constant-Time *J*-Resolved Approach

Giuseppe Melacini*

Contribution from the Department of Chemistry & Biochemistry, University of California at San Diego, 9500 Gilman Drive, La Jolla, California 92093

Received May 10, 2000. Revised Manuscript Received July 14, 2000

Abstract: The NMR methods used to characterize molecular interactions through NOEs rely on isotope editing/filtering strategies designed to select for/against $^{13}C(^{15}N)$-bound proton spins. The filter efficiency depends critically on the optimal compensation for variations in J_{CH} scalar coupling constants, which is effectively obtained by the currently available second- and third-order isotope filters but at the cost of losing all intramolecular NOEs. Here a new filtering/editing strategy based on quadrature-free constant-time *J*-spectroscopy is presented that achieves J_{CH}-compensation and the simultaneous measurement of inter- and intramolecular NOEs between ^{13}C-bound ^{1}H spins. The *J*-resolved frequency dimension is incorporated in a semiconstant-time NOESY-HSQC experiment resulting in a 4D spectrum in which signals arising from protons bound to ^{13}C (or ^{15}N) are separated from those originating from protons bound to ^{12}C (or ^{14}N) nuclei. The filter performance does not depend on double tuning of delays or on empirical correlations. In addition, the filter efficiency is not limited by upper bounds on the J_{CH} values. The large *J*-bandwidth and the substantial time-saving make the pulse sequence here outlined a valuable tool for investigating noncovalent molecular assemblies by NMR, especially in the context of fast structural elucidations required for the development of structural genomics.

Introduction

Biological function is closely related to the noncovalent assembly of macromolecules in solution and high-resolution NMR spectroscopy is a valuable tool to investigate such interactions. Specifically, the NMR methods used to characterize high-affinity macromolecular complexes rely on the selective (^{15}N,^{13}C) labeling of one of the interacting partners and on isotope editing/filtering techniques to select for/against protons that are one-bond coupled to ^{15}N or ^{13}C spins.[1,2] While the editing process is extremely effective, the filtering efficiency depends critically on the optimal compensation for variations in J_{CH} scalar coupling constants, which vary over a wide range (approximately 120−220 Hz). The required *J*-compensation can be elegantly obtained by the currently available high-order isotope filters that allow the passage of proton coherence only if J_{CH} is lower than a chosen threshold.[2−7] In addition, second-order filters[2−4] have been significantly enhanced through the use of adiabatic ^{13}C inversion pulses with a sweep rate tuned to the J_{CH} vs ^{13}C chemical shift profile.[5,6] Furthermore, third-order filters have been proposed based on the isomorphism between broadband polarization transfer and composite pulse rotations resulting in high suppression efficiency for J_{CH} values in the 115−165 Hz range.[7]

A drawback of both second- and third-order filters is that the high filtering performance is obtained at the cost of losing all intramolecular NOEs of the labeled macromolecule. This is because the proton magnetization originating from $^{1}H-^{13}C$ (and $^{1}H-^{15}N$) pairs is channeled into heteronuclear zero- and double-quanta which are not transformed into observable coherence. Here a new filtering/editing strategy based on *J*-spectroscopy[8] is presented that achieves J_{CH}-compensation and the simultaneous measurement of inter- and intramolecular NOEs between

* Fax: (858) 534-0130. E-mail: gm@chem.ucsd.edu.

(1) (a) Otting, G.; Senn, H.; Wagner, G.; Wüthrich, K. *J. Magn. Reson.* **1986**, *85*, 500−505. (b) Otting, G.; Wüthrich, K. *J. Magn. Reson.* **1989**, *85*, 586. (c) Wider, G.; Weber, C.; Traber, H.; Widmer, H.; Wüthrich, K. *J. Am. Chem. Soc.* **1990**, *112*, 9015−9016. (d) Otting, G.; Wüthrich, K. *Q. Rev. Biophys.* **1990**, *23*, 39−96. (e) Folkers, P. J. M.; Folmer, R. H. A.; Konings, R. N. H.; Hilbers, C. W. *J. Am. Chem. Soc.* **1993**, *115*, 3798−3799. (f) Burgering, M. J. M.; Boelens, R.; Kaptein, R. *J. Biomol. NMR* **1993**, *3*, 709. (g) Folkers, P. J. M.; Nilges, M.; Folmer, R. H. A.; Konings, R. N. H.; Hilbers, C. W. *J. Mol. Biol.* **1994**, *236*, 229. (h) Bax, A.; Grzesiek, S.; Gronenborn, A. M.; Clore, M. G. *J. Magn. Reson. Ser. A* **1994**, *106*, 269. (i) Folmer, R. H. A.; Hilbers, C. W.; Konings, R. N. H.; Hallenga, K. *J. Biomol. NMR* **1995**, *5*, 427. (j) Yang, J. C.; Ramesh, V.; Roberts, G. C. K. *J. Magn. Reson. Ser. B* **1995**, *106*, 284. (k) Emetarom, C.; Hwang, T. L.; Mackin, G.; Shaka, A. J. *J. Magn. Reson. Ser. A.* **1995**, *115*, 137−140. (l) Breeze, A. L.; Kara, B. V.; Barratt, D. G.; Anderson, M.; Smith, J. C.; Luke, R. W.; Best, J. R.; Cartlidge, S. A. *Embo J.* **1996**, *15(14)*, 3579−3589.

(2) (a) Sattler, M.; Schleucher, J.; Griesinger, C. *Prog. NMR Spectrosc.* **1999**, *34*, 93−158. (b) Breeze, A. *Prog. NMR Spectrosc.* **2000**, *36*, 323−372.

(3) Kogler, H.; Sorensen, O. W.; Bodenhausen, G.; Ernst, R. R. *J. Magn. Reson.* **1983**, *55*, 157.

(4) (a) Ikura, M.; Bax, A. *J. Am. Chem. Soc.* **1992**, *114*, 2433−2440. (b) Gemmecker, G.; Oleiniczak, E. T.; Fesik, S. W. *J. Magn. Reson.* **1992**, *96*, 199−204. (c) Petros, A. M.; Kawai, M.; Luly, J. R.; Fesik, S. W. *FEBS Lett.* **1992**, *308*, 309. (d) Lee, W.; Revington, M. J.; Arrowsmith, C.; Kay, L. E. *FEBS Lett.* **1994**, *350*, 87−90. (e) Xu, R. X.; Gampe, R. T.; Davis, D. G. *J. Magn. Reson. Ser. B* **1994**, *105*, 180. (f) Ogura, K.; Terasawa, H.; Inagaki, F. *J. Biomol. NMR* **1996**, *8*, 492. (g) Dalvit, C.; Ramage, P.; Hommel, U. *J. Magn. Reson.* **1998**, *131*, 148. (h) Dalvit, C.; Cottens, S.; Ramage, P.; Hommel, U. *J. Biomol. NMR* **1999**, *13*, 43.

(5) Kupce, E.; Freeman, R. *J. Magn. Reson.* **1997**, *127*, 36−48.

(6) Zwahlen, C.; Legault, P.; Vincent, S. J. F.; Greenblatt, J.; Konrat, R.; Kay, L. E. *J. Am. Chem. Soc.* **1997**, *119*, 6711−6721.

(7) Stuart, A. C.; Borzilleri, K. A.; Withka, J. M.; Palmer, A. G., III. *J. Am. Chem. Soc.* **1999**, *121*, 5346−5347.

10.1021/ja0015996 CCC: $19.00
Published on Web 09/23/2000

^{13}C-bound ^{1}H spins. The filter performance does not depend on double tuning of delays[3,4] nor on empirical correlations.[5,6] In addition, it is not limited by upper bounds on the J_{CH} values.[7] The novel filtering/editing principle is verified using a modified NOESY-(^{1}H,^{13}C) HSQC, which was applied to the complex of (^{15}N,^{13}C) labeled RIIα(1−44) and unlabeled Ht31(493−515) illustrating the utility of the proposed method.[9]

Theory

In a *J*-resolved spectrum the ^{13}C-bound ^{1}H spins appear at $\pm J_{CH}/2$ Hz in the indirectly detected dimension, while the ^{12}C-bound protons resonate at zero frequency offset because they are not *J*-modulated in the time domain. This property offers the rationale for the separation of inter- and intramolecular NOEs, provided that the spectral width along the *J*-dimension is larger than J_{CH} and that the signals at $\pm J_{CH}/2$ Hz are resolved from the peaks at 0 Hz. To fulfill the latter requirement independently of relaxation properties, a constant-time (CT) version[10] of the *J*-resolved experiment is adopted (Figure 1a). In the CT experiment the line shape is determined by the window function used to ensure smooth apodization of the truncated interferogram, while the resolution depends on the total length of the CT period (2λ in Figure 1a). In addition, the resolution of the CT scheme can be significantly enhanced by mirror image linear prediction[11] thus minimizing the CT duration necessary to resolve peaks at $\pm J_{CH}/2$ Hz from those at zero offset.

The CT-J resolved (CT-J) pulse sequence element (Figure 1a) was implemented using two adiabatic ^{13}C inversions[12] characterized by a total sweep range that is large in comparison with the radio frequency field intensity (see Materials and Methods). The spin inversion can thus be approximated to occur when the frequency sweep passes through the chemical shift of a given spin or group of spins.[5] Considering that the two adiabatic pulses are applied with opposite sweep directions (Figure 1a),[5] it is then simple to prove through product operator algebra[13] (Supporting Information) that at instant *a* (Figure 1a) the effective time for the one-bond ^{13}C−^{1}H scalar coupling (J_{CH}) evolution is simply t_n (Figure 1a), which is a generic incremented delay of a multidimensional pulse sequence. In addition, the symmetry of the 90° ^{1}H pulses with respect to the 180° ^{1}H pulse in Figure 1a ensures that at time point *a* the chemical shift evolution is refocused. The coherence of a generic proton "I" at time *a* in Figure 1a is then described by

$$-I_y \exp[-2(\Delta + \tau_{Ad} + \lambda)/T_2] \cos(\pi J_{CH} t_n) \qquad (1)$$

where the single T_2 decay time constant approximates the average effect of the relaxation rates for in-phase and anti-phase single-quantum proton coherences present during the CT-J block. Other operators different from that described in eq 1 are

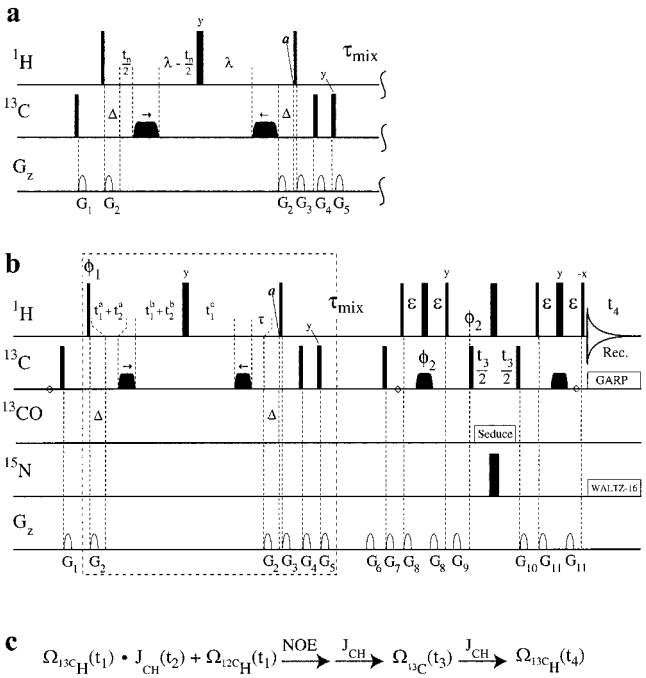

Figure 1. Pulse sequences for the simultaneous editing and *J*-compensated filtering based on the quadrature-free constant-time *J*-resolved (CT-J) method. Narrow (wide) rectangles represent hard 90° (180°) pulses. The rounded trapezoids correspond to adiabatic ^{13}C WURST[5,12] pulses (see Materials and Methods). No arrows or an arrow from left to right indicates a sweep from upfield to downfield while the other arrow denotes an opposed adiabatic sweep. The delay Δ is set to 0.353 ms. (a) Basic CT-J element where t_n represents a generic incremented delay, while λ is a constant delay that determines the maximum resolution along the CT-J dimension ($t_{n,max} = 2\lambda$). (b) 4D F1 semiconstant time, F2 CT-J, F3 ^{13}C-edited NOESY-HSQC. This pulse sequence is designed for the simultaneous detection of inter- and intramolecular NOEs in D_2O. The diamonds in the ^{13}C channel indicate changes of ^{13}C carrier frequency, which is first set at 67 ppm then shifted to 40 ppm at the end of the NOE mixing time and restored at 67 ppm before GARP[17] decoupling. The delays t_2^a and t_2^b implement the CT-J resolution in F2: $t_2^a = 3\ \mu s + [n/(2SW_2)]$ and $t_2^b = 3\ \mu s + \lambda - [n/(2SW_2)]$, where SW_2 is the spectral width (SW) for the F2 dimension (312.5 Hz) and $n = 0, 1, ..., N-1$ ($t_2 = n/SW_2$). *N* is the total number of real (r) t_2 points ($N = 4$ for $\lambda = 4.81$ ms). No quadrature scheme is needed for the CT-J dimension (F2). The delays t_1^a, t_1^b, and t_1^c are related to the semi-CT ^{1}H frequency labeling in F1: $t_1^a = 3\ \mu s + [m/(2SW_1)]$, $t_1^b = 3\ \mu s + [(0.5/SW_1) - (\lambda/M)]m$, and $t_1^c = 6\ \mu s + \lambda - (\lambda/M)m$, where SW_1 is the SW for the F1 dimension and $m = 0, 1, ..., M-1$ ($t_1 = m/SW_1$). *M* is the total number of complex (c) t_1 points. The delay τ_{mix} defines the NOE mixing time, while τ and ϵ are set to 6 μs and 1.785 ms, respectively. The gradient pulses are shaped according to the center sine band and are 0.50 ms long except for G_2 and G_5, which last 0.20 and 0.87 ms, respectively. Every gradient pulse is followed by a delay of at least 0.15 ms. The relative gradient strengths are the following: G_1 −1.75, G_2 1.34, G_3 −2.78, G_4 −3.81, G_5 −2.78, G_6 −1.86, G_7 −1.62, G_8 1.00, G_9 3.40, G_{10} −2.44, and G_{11} 1.16. Phases are "*x*" unless otherwise specified. Phase cycle: $\phi_1 = x, -x$; $\phi_2 = x, x, -x, -x$; rec = $x, -x, -x, x$. (c) Scheme showing which Hamiltonian evolves during which delay.

(8) (a) Aue, P. W.; Karhan, J.; Ernst, R. R. *J. Chem. Phys.* **1976**, *64*, 4226. (b) Bodenhausen, G.; Freeman, R.; Niedermeyer, R.; Turner, D. L. *J. Magn. Reson.* **1976**, *24*, 291. (c) Müller, L.; Kumar, A.; Ernst, R. R. *J. Magn. Reson.* **1977**, *25*, 383. (d) Nagayama, K.; Bachmann, P.; Wüthrich, K.; Ernst, R. R. *J. Magn. Reson.* **1978**, *31*, 133. (e) Vuister, G.; Boelens, R. *J. Magn. Reson.* **1987**, *73*, 328−333.

(9) (a) Newlon, M. G.; Roy, M.; Morikis, D.; Hausken, Z. E.; Coghlan, V.; Scott, J. D.; Jennings, P. A. *Nat. Struct. Biol.* **1999**, *3*, 222−227. (b) Newlon, M. G.; Roy, M.; Morikis, D.; Hausken, Z. E.; Coghlan, V.; Scott, J. D.; Jennings, P. A. Submitted for publication. (c) Newlon, M. G. Ph.D. Thesis, University of California San Diego, La Jolla, 1999, pp 105−163.

(10) (a) Bax, A.; Mehlkopf, A. F.; Smidt, J. *J. Magn. Reson.* **1979**, *35*, 167−169. (b) Bax, A.; Freeman, R. *J. Magn. Reson.* **1981**, *44*, 542−561. (c) Rance, M.; Wagner, G.; Sørensen, O. W.; Wüthrich, K.; Ernst, R. R. *J. Magn. Reson.* **1984**, *59*, 250−261. (d) Powers, R.; Groenenborn, A. M.; Clore, G. M. Bax, A. *J. Magn. Reson.* **1991**, *94*, 209. (e) Van de Ven, F. J. M.; Philippens, M. E. P. *J. Magn. Reson.* **1992**, *97*, 637−644. (f) Santoro, J.; Bruix, M.; Gonzalez, C.; Nieto, J. L.; Rico, M. *J. Biomol. NMR* **1992**, *2*, 647−653. (g) Vuister, G.; Delaglio, F.; Bax, A. *J. Biomol. NMR* **1993**, *3*, 67−80. (h) Ottiger, M.; Delaglio, F.; Marquardt, J.; Tjandra, N.; Bax, A. *J. Magn. Reson.* **1998**, *134*, 365−369. (i) Melacini, G.; Boelens, R.; Kaptein, R. *J. Biomol. NMR* **1999**, *15* (3), 189−201.

(11) Zhu, G.; Bax, A. *J. Magn. Reson.* **1990**, *90*, 405−410.

(12) (a) Bohlen, J. M.; Bodenhausen, G. *J. Magn. Reson., A* **1993**, *102*, 293. (b) Kupce, E.; Freeman, R. *J. Magn. Reson., A* **1995**, *115*, 273−276.

(13) (a) Sørensen, O. W.; Eich, G. W.; Levitt, M. H.; Bodenhausen, G.; Ernst, R. R. *Prog. NMR Spectrosc.* **1983**, *16*, 163−192. (b) Van de Ven, F. J. M.; Hilbers, C. W. *J. Magn. Reson.* **1983**, *54*, 512−520.

dephased by the gradients present during the NOE mixing period (Figure 1a). No quadrature detection is employed for t_n in the CT-J element and therefore the spectrum obtained after complex Fourier transform is symmetrical with respect to the line Fn = 0 Hz, where Fn denotes the frequency dimension related to t_n. Both symmetric halves are characterized by an absorptive line shape because the two adiabatic pulses with opposite sweep directions[5] ensure that no net J_{CH} evolution occurs for the first acquired t_n point thus avoiding phase corrections. If proton I is bound to a ^{13}C nucleus, it will appear at F$n = \pm J_{CH}/2$ Hz. If proton I is bound to a ^{12}C nucleus, J_{CH} is formally zero and it will appear at Fn = 0 Hz, as desired for the purpose of separating inter- and intramolecular NOEs.

The CT-J strategy was then combined with semi-CT chemical shift evolution[14] (Figure 1b) that results in enhanced resolution for the indirect ^{1}H frequency labeling dimension. In the boxed region of Figure 1b the delays t_2^a and t_2^b implement the CT J-resolution along F2 (vide supra), while the delays t_1^a, t_1^b, and t_1^c are related to the semi-CT ^{1}H chemical shift evolution in F1. Specifically, simple product operator formalism[13] computations (Supporting Information) show that at instant a in Figure 1b the effective times for the evolution of Ω_H, J_{CH}, and for transverse relaxation (τ_{Tr}) are respectively equal to t_1, t_2, and ($\alpha + \beta t_1$), where α and β are constants given by $\alpha = 2(\Delta + \tau_{Ad} + \lambda + 12\ \mu s)$ and $\beta = [1 - (2\lambda SW_1/M)]$ (Figure 1b); SW_1 is the spectral width for the F1 dimension and M is the total number of complex t_1 points. At time point a of Figure 1b the coherence of a generic proton "I" is therefore described by

$$-I_y \cos(\Omega_H t_1) \exp[-(\alpha + \beta t_1)/T_2] \cos(\pi J_{CH} t_2) \qquad (2)$$

Again the other operators are dephased by the gradients present during the NOE mixing period. In eq 2, the terms in t_1 encode for the semi-CT frequency labeling along F1, while the amplitude modulation in t_2 is the basis for the CT-J resolved separation of intra- and intermolecular NOEs, as discussed above. The remaining part of the pulse sequence after point a includes an NOE mixing period and an HSQC block[6,7] with evolution of the ^{13}C and ^{13C}H chemical shifts during t_3 and t_4, respectively (Figure 1b). The pulse sequence of Figure 1b results therefore in a 4D spectrum where J_{CH} is resolved in F2 while the $^{12C+13C}$H, ^{13}C, and ^{13C}H spins are frequency labeled in F1, F3, and F4, respectively (Figure 1c). The 4D scheme thus incorporates the CT-J dimension in the semiconstant time 3D NOESY-HSQC experiment and signals arising from protons bound to ^{13}C nuclei can be resolved from those originating from protons bound to ^{12}C nuclei. The CT-J approach is also applicable to the separation of ^{15}N-bound and ^{14}N-bound ^{1}H spins, as described in the Supporting Information.

Materials and Methods

Data Acquisition. All experiments were run on a Bruker DMX500 NMR spectrometer using as sample the complex of ^{15}N,^{13}C-labeled RIIα(1−44) and unlabeled Ht31(493−515) at 25 °C and in D_2O prepared as previously described.[9] The ^{1}H pulses are centered on the HDO resonance. The adiabatic ^{13}C WURST[5,12] pulses were characterized by a $B_{1,max} = 8.4$ kHz, a duration of $\tau_{Ad.} = 500\ \mu s$, and a sweep range of 60 kHz centered at 67 ppm. A trim spin-lock can be used in the HSQC block of Figure 1c to improve water suppression.[15] The SEDUCE carbonyl decoupling[16] was implemented as indicated in ref 6. The GARP[17] ^{13}C decoupling had a strength of 3.7 kHz. The ^{15}N pulses in Figure 1b are not necessary if $t_{3,max}$ and $t_{4,max}$ are short enough to avoid resolution of the scalar couplings to ^{15}N spins. A relaxation delay of 1 s was used for all experiments. Quadrature in F1 and F3 was obtained via States-TPPI[18] on ϕ_1 and ϕ_2 (Figure 1b), respectively, while the implementation of the quadrature-free CT-J block requires only a single loop used to increment and decrement the delays t_2^a and t_2^b, respectively (Figure 1b). As compared to the nested loops corresponding to the other indirectly detected dimensions in the 4D experiment, the CT-J loop is the fastest (most internal). In the 3D experiments of Figures 2 and 3a,c, 512(c) × 4(r) × 256(c) t_4, t_2, and t_1 points were recorded for spectral widths (SWs) of 8012.8 × 312.5 × 6000.0 Hz, respectively. In the 2D experiment of Figure 3b,d, 512-(c) × 256(c) t_3 and t_1 points were acquired for SWs of 8012.8 × 6000.0 Hz, respectively. In the 4D experiment of Figure 3e,f, 256(c) × 32(c) × 4(r) × 100(c) t_{4-1} points were recorded for SWs of 4845.0 × 3750.1 × 312.5 × 4808.2 Hz, respectively. The total acquisition time for the 4D experiment was 89 h. The other experimental details are as described in the figure captions.

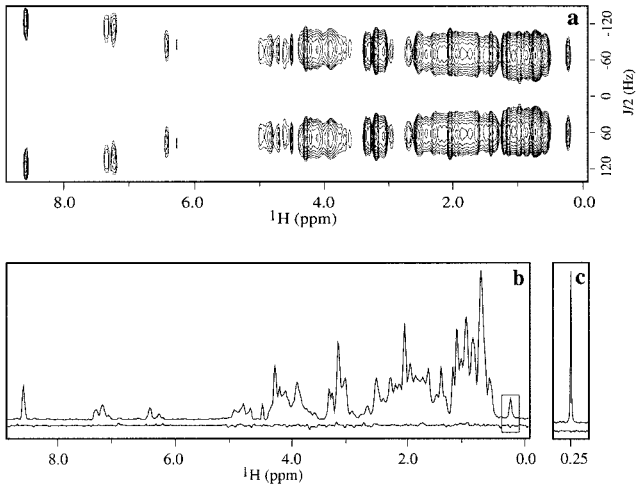

Figure 2. Spectra from a 3D data matrix acquired using the pulse sequence of Figure 1b with $\tau_{mix} = 4.4$ ms. The t_3 period was not incremented and a 180°$_y$(^{13}C) refocusing pulse was inserted in the middle of t_3 thus avoiding ^{13}C frequency labeling. Four t_2 real points were acquired with $\lambda = 4.81$ ms. (a) First CT-J 2D (F2,F4) plane. (b) Plot of the intensity at $J/2$ Hz (top) and at 0 Hz (bottom) offsets in spectrum a. (c) Horizontal traces corresponding to the boxed high-field region in panel b. These traces were extracted from the (F1,F4) NOE planes at $J/2$ = 70 Hz (top) and at J = 0 Hz (bottom). All compared spectra are scaled to the same noise level.

Data Processing. In the processing of the 4D data matrix acquired using the pulse sequence of Figure 1b linear prediction with respect to t_2 typically occurs after the other dimensions (t_1, t_3, t_4) are Fourier transformed. The processing of the t_1, t_3, t_4 dimensions is as for typical NOESY-HSQC data matrices.[6] As to the t_2 J-dimension, when four real t_2 points are acquired a third-order mirror-image linear prediction is employed to enhance resolution. Linear prediction is followed by multiplication by a squared cosine window function to ensure a smooth ending of the J-interferogram to a zero value. The first t_2 point is multiplied by a 0.5 correction factor. Zero filling and complex Fourier transform follow. No phase corrections are necessary either in F2 or in F1, while 90°, −180° zero- and first-order phase corrections, respectively, are applied in the aliased ^{13}C F3 dimension. All spectra were processed using NMRPipe[19] and analyzed using Felix97 (Molecular Simulation, Inc.).

(14) Grzesiek, S.; Bax, A. *J. Biomol. NMR* **1993**, *3*, 185−204.
(15) (a) Otting, G.; Wüthrich, K. *J. Magn. Reson.* **1988**, *76*, 569−574. (b) Messerle, B. A.; Wider, G.; Otting, G.; Weber, C.; Wüthrich, K. *J. Magn. Reson.* **1989**, *85*, 608−613.
(16) McCoy, M.; Mueller, L. *J. Magn. Reson.* **1993**, *101*, 122−130.
(17) Shaka, A. J.; Barker, P. B.; Freeman, R. *J. Magn. Reson.* **1985**, *64*, 547−552.
(18) Marion, D.; Ikura, M.; Tschudin, R.; Bax, A. *J. Magn. Reson.* **1989**, *85*, 393−399.
(19) Delaglio, F.; Grzesiek, S.; Vuister, G. W.; Zhu, G.; Pfeifer, J.; Bax, A. J. *Biomol. NMR* **1995**, *6* (3), 277−293.

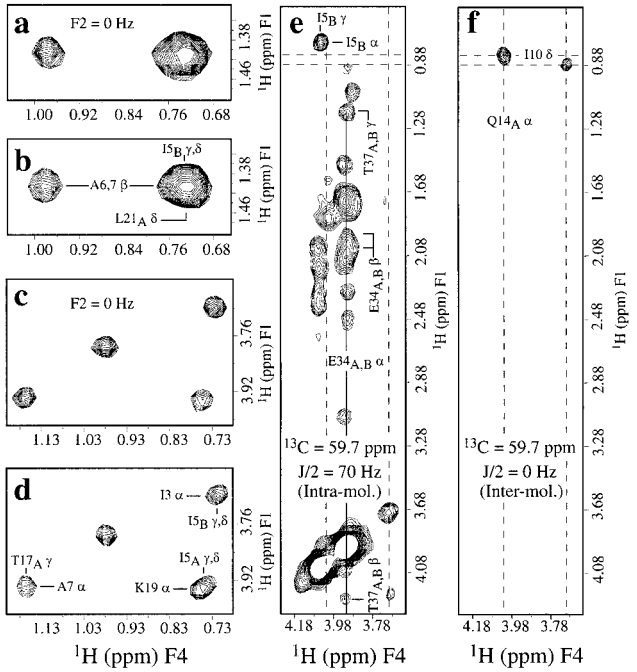

Figure 3. (a, c) Representative expansions from the (F1,F4) NOE plane at $J = 0$ Hz extracted from a 3D spectrum recorded as the matrix of Figure 2 but with $\tau_{mix} = 149$ ms. The number of scans is 16. (b, d) Same expansions as panels a and c but for the control F1 ^{13}C-filtered, F2 ^{13}C-edited NOESY-HSQC acquired using the pulse sequence of ref 7 with 64 scans and $\tau_{mix} = 149$ ms. The ^{13}C chemical shift evolution is refocused as described in the caption of Figure 2. Panels a−d are plotted with the same threshold and contouring parameters. (e) Spectral region from the (F1,F4) NOE plane at $J/2 = 70$ Hz (F2) and at $\delta(^{13}C) = 59.7$ ppm (F3) extracted from a 4D spectrum acquired using the pulse sequence of Figure 1b with $\tau_{mix} = 149$ ms. (f) As panel e but extracted at $J/2 = 0$ Hz. The dashed lines in panel f indicate the F1 and F4 $\delta(^1H)$ values corresponding to intermolecular NOEs. The same lines are reported in panel e to facilitate comparisons. Assignments are provided for cross-peaks devoid of overlap-related ambiguities in the 4D spectrum. The assignments[9] for the dimeric RIIα(1−44) are indicated using the one-letter codes for the amino acids, followed by the residue number, the monomer specification (A or B), and the atom name. The assignments for the Ht31(493−515) peptide are denoted with the same nomenclature but without the monomer specification. For isoleucine residues ("I") the atom name "γ" indicates the methyl γ protons. The assignments in panels a and c are the same as those in panels b and d. See also Supporting Information (Figure 3.supp) for further details on the assignment in panels a−d.

Results and Discussion

The proposed experiment (Figure 1b) was validated using the complex of ^{15}N,^{13}C-labeled RIIα(1−44) and unlabeled Ht31(493−515). Ht31(493−515) is an A-kinase-anchoring peptide that binds with nanomolar affinity the RIIα(1−44) fragment of the 3′,5′-cyclic monophosphate (cAMP)-dependent protein kinase (PKA).[9] This interaction is crucial for PKA localization and occurs through an extended hydrophobic surface formed by the antiparallel I and I′ helices of dimeric RIIα(1−44).[9,20]

Data were first recorded with a short NOE mixing time (4.4 ms) so no significant incoherent transfer of magnetization occurs and the filtering quality of the CT-J element can be directly assessed by measuring the residual signal at F2 = 0 Hz. The delay λ was set to 4.81 ms resulting in a CT-J block not longer than the previously reported third-order filter.[7] Four real t_2 points were acquired for a spectral width of 312.5 Hz leading to a mirror-image linear predicted *J*-spectrum with good resolution (Figure 2a). The signal at F2 = 0 Hz is reduced by an average factor of 97.6% relative to that at F2 = $J_{CH}/2$ Hz (Figure 2b). Clean filtering is obtained even for the high-field methyl characterized by short J_{CH} values (Figure 2c). Furthermore the *J*-bandwidth of the filter is extended to all aromatic residues, including the large J_{CH} values (∼200−220 Hz) of the histidine imidazole group (Figure 2a,b).

To further corroborate the pulse sequence of Figure 1b a reference spectrum was measured using the previously published third-order *J*-compensated isotope filter[7] with $\tau_{mix} = 149$ ms and with no ^{13}C evolution. The observed cross-peak patterns in this control experiment (Figure 3b,d) are very similar to those detected in the matrix acquired using the CT-J based scheme of Figure 1b (Figure 3a,c) in exactly the same recording time. In addition, the CT-J pulse sequence (Figure 1b) allows the simultaneous measurement of the intramolecular NOEs between ^{13}C-bound ^{1}H spins, as demonstrated by Figure 3e,f. This figure shows (F1,F4) ^{1}H−^{1}H NOE planes extracted from a 4D spectrum at the same ^{13}C (F3) frequency but at different values in the *J* dimension (F2). In Figure 3e, $J/2 = 70$ Hz and intramolecular NOEs are observed between protons of labeled RIIα(1−44), while in Figure 3f, $J = 0$ Hz and intermolecular NOEs are detected from unlabeled Ht31(493−515) to labeled RIIα(1−44).

Conclusion

A novel isotope filtering method has been developed based on the CT-J principle resulting in a large *J*-bandwidth and in substantial time saving by allowing the simultaneous measurement of intra- and intermolecular NOEs. These features make the 4D pulse sequence here outlined a valuable tool for the investigation of noncovalent molecular assemblies by NMR, especially in the context of fast structural elucidations required for the development of structural genomics.

Acknowledgment. This paper is dedicated to Marialuisa and Guido Badaloni. Dr. P. A. Jennings, Dr. M. G. Newlon, and Dr. M. Roy are gratefully acknowledged for providing the RIIα-Ht31 sample (NIH-DK54441-PAJ) together with Dr. E. A. Komives, Dr. S. S. Taylor (UCSD), and Dr. M. Tessari (Nijmegen University, NL) for helpful discussions. I thank Dr. J. M. Wright for expert engineering assistance and Dr. J. Craven for sharing the "Clipper" program to display NMR pulse sequences. Finally, I thank the reviewers for constructive comments.

Supporting Information Available: Further details on eqs 1 and 2; extension to samples in ^1H_2O; and planes from the 4D spectrum used to confirm the assignments in Figure 3a−d (PDF). This material is available free of charge via the Internet at http://pubs.acs.org.

JA0015996

(20) Newlon, M. G.; Roy, M.; Hausken, Z. E.; Scott, J. D.; Jennings, P. A. *J. Biol. Chem.* **1997**, *272*, 23637−23644.